Supporting Information for "Heterogeneous Land-Surface Effects on TKE and Cloud Formation: Statistical Insights from LES Cases"

Jason S. Simon[1,2], Andrew D. Bragg[1], and Nathaniel W. Chaney[1]

[1]Duke University, Durham, NC, USA

[2]Present Address: Saint Augustine's University, Raleigh, NC, USA

Contents of this file

1. WRF Model Description

2. HydroBlocks Model Description

3. Figures S1 to S5

Introduction

Information here consists of extended model descriptions, additional results which may be of interest to the reader, and a demonstration of the land-surface filtering method used in the primary document.

————

August 13, 2023, 8:17pm

WRF Model Description

Large-eddy simulations are conducted using a modification of version 3.8.1 of the WRF model (Skamarock et al., 2008). Changes implemented, maintained, and distributed by the LES ARM Symbiotic Simulation and Observation Workflow (LASSO) campaign (Endo et al., 2015; W. Gustafson et al., 2019; W. I. Gustafson et al., 2020) notably include the addition of specified large-scale tendency terms and enhanced output fields. An additional modification implemented by Simon, Bragg, Dirmeyer, and Chaney (2021) is also used here to specify heterogeneous surface properties from an offline LSM.

Each case is run with heterogeneous and homogeneous land-surface fields. Heterogeneous land-surface cases use solutions from the HydroBlocks LSM to specify two-dimensional, time-evolving surface fields for sensible heat flux, latent heat flux, skin temperature (found via specified emissivity and upward longwave radiation fields), albedo, and momentum drag coefficient. The homogeneous cases specify a uniform (in space) surface of each field to match the time-evolving domain-wide mean of the corresponding heterogeneous case (skin temperature is diagnosed from mean values of upward longwave radiation and emissivity, rather than a domain-average of skin temperature directly). There is no feedback from the atmosphere to the land surface in the LES; the HydroBlocks LSM is run offline and the output surface fields are specified as the bottom boundary in the WRF model. Histograms of means and standard deviations of mid-day latent and sensible heat flux fields are shown in Fig. S1.

Following the LASSO configuration, simulations use the Thompson graupel microphysics scheme and the RRTMG radiation scheme (though surfaces are specified offline

by HydroBlocks) with the cumulus and PBL schemes turned off. The model timestep is 0.5 s. The domain is approximately 14.5 km tall with 227 vertical levels and a vertical resolution of 30 m in the lower 5 km of the column. Periodic boundary conditions are used in both lateral directions and a w-Rayleigh damping layer is applied in the upper 2 km of the column. The LES domain uses a flat bottom boundary, though terrain is considered by the offline HydroBlocks simulation for subsurface and surface routing. Initial profiles for potential temperature, water vapor mixing ratio, and lateral velocity components are obtained from the LASSO database and are applied uniformly to the domain. Large-scale heat and moisture tendency profiles based on the VARANAL dataset, obtained from the LASSO database and configuration, are also included. The model configuration is otherwise the same as in Simon et al. (2021), which is in turn largely based on the LASSO configuration.

HydroBlocks Model Description

HydroBlocks is a field-scale resolving land-surface model (Chaney, Metcalfe, & Wood, 2016) that accounts for the water, energy, and carbon balance to solve land-surface processes at field scales (30 m) over regional to continental extents (Chaney, Metcalfe, & Wood, 2016; Chaney et al., 2020; Vergopolan et al., 2020). The core of HydroBlocks is the Noah-MP vertical land surface scheme (Niu et al., 2011). For this study, HydroBlocks is spun up for two years and uses high-resolution (30 m) soil type and land cover maps from the Probabilistic Remapping of SSURGO (POLARIS) (Chaney, Wood, et al., 2016; Chaney et al., 2019) and National Land Cover Database (NLCD) (Homer et al., 2012) datasets, respectively, and one-eighth degree NLDAS-2 meteorology (Cosgrove

et al., 2003; Mitchell et al., 2004) with NCEP Stage-IV radar rainfall ($\sim$4 km) data (Lin

& Mitchell, 2005). The hourly state of the land surface produced by HydroBlocks for

the period of interest is then used to specify surface values in the WRF model. For

consistency, surface-flux fields are adjusted so that the domain-wide averages match the

time-evolving scalar surface fluxes specified by the LASSO campaign, which are from the

observationally-improved VARANAL dataset.

Additional Fields

The analysis shown in Sec. 3.2 of the primary text for χ and γ(LWP) compared to statistics of the surface sensible heat flux field, H, is repeated here for γ(TKE) compared to statistics of H in Fig. S2. The correlations between γ(TKE) and mean values of $\sigma(H)$, $L_\Delta(H)$, $L_2(H)$ are not appreciably different than the correlations between χ and the same statistics of the H field, particularly when considering $\sigma(H)$. There is a small, but nontrivial, negative Pearson correlation between γ(TKE) and $\mu(H)$, where $\rho_p = -0.22$ (Fig. S2a), which is understood by recalling that γ(TKE) is the ratio of TKE in corresponding heterogeneous and homogeneous cases. Thus, larger mean surface sensible heat flux values reduce the relative significance of TKE generated by any heterogeneous surface patterns, making the total TKE more comparable between heterogeneous and homogeneous cases. Indeed, this negative correlation is virtually eliminated when comparing only the circulating components of TKE (χ) to $\mu(H)$, where $\rho_p = 0.00$ (Fig. 3a in the main text).

The same analysis for χ, γ(LWP), and γ(TKE) compared to statistics of the surface latent heat flux field, Q, is shown in Fig. S3. The relationships between the χ, γ(LWP), and γ(TKE) metrics and the surface latent heat flux field are very similar to those seen for the surface sensible heat flux field, both quantitatively and qualitatively. The only notable difference between the two surface fields is that the correlation between γ(TKE) and $\mu(Q)$ is positive rather than the negative correlation seen for $\mu(H)$, though the two are similar in magnitude. The small positive correlation between γ(TKE) and $\mu(Q)$ (Fig. S3a) appears logical, as a larger mean latent heat flux would not be expected to inherently generate

TKE in the atmosphere but may increase cloud production rates and thus exaggerate heterogeneous surface effects.

The relationships between χ, $\gamma(\text{LWP})$, and $\gamma(\text{TKE})$ compared to statistics of the surface temperature field, T, do show some distinctive features relative to those with H and Q (Fig. S4). The relationships between the atmospheric metrics and $\sigma(T)$ is very similar to those seen for $\sigma(H)$ and $\sigma(Q)$, but there is a larger correlation between $\mu(T)$ and all three atmospheric metrics, particularly χ (Fig. S4a), than is seen for $\mu(H)$ or $\mu(Q)$. This suggests that while mean energy flux values do not correlate with the development of secondary circulations, larger mean surface temperatures may help in circulation development. As well, both length-scale metrics, $L_\Delta(T)$ and $L_2(T)$, show a lower correlation with the atmospheric metrics than the length scales calculated from H or Q, suggesting that the spatial structures of surface heat fluxes are more related to the atmospheric response than the spatial structures of surface temperature. Intuitively, it should be the case that the surface flux fields have a more direct impact on the atmosphere than surface temperature; the surface sensible and latent heat fluxes directly connect the land-surface to the atmosphere whereas the surface temperature is connected to the atmosphere via the surface heat fluxes.

Example Filtered Fields

The filter used in Sec. 3.3 of the primary text, defined as

$$F = 1 - \exp\left[-2\pi^2 \left(\frac{\Delta_{\text{filter}}}{\lambda}\right)^2\right], \tag{1}$$

where Δ_{filter} is the nominal filter length, is shown as applied to a representative mid-day sensible heat flux field at an increasingly fine filter length in Fig. S5.

References

Chaney, N. W., Metcalfe, P., & Wood, E. F. (2016). HydroBlocks: a field-scale resolving land surface model for application over continental extents. *Hydrological Processes*, *30*(20), 3543-3559. doi: 10.1002/hyp.10891

Chaney, N. W., Minasny, B., Herman, J. D., Nauman, T. W., Brungard, C. W., Morgan, C. L., ... Yimam, Y. (2019). POLARIS soil properties: 30-m probabilistic maps of soil properties over the contiguous United States. *Water Resources Research*, *55*(4), 2916–2938.

Chaney, N. W., Torres-Rojas, L., Vergopolan, N., & Fisher, C. K. (2020). Two-way coupling between the sub-grid land surface and river networks in Earth system models. *Geoscientific Model Development Discussions*, *2020*, 1–31. doi: 10.5194/gmd-2020-291

Chaney, N. W., Wood, E. F., McBratney, A. B., Hempel, J. W., Nauman, T. W., Brungard, C. W., & Odgers, N. P. (2016). POLARIS: A 30-meter probabilistic soil series map of the contiguous United States. *Geoderma*, *274*, 54–67.

Cosgrove, B. A., Lohmann, D., Mitchell, K. E., Houser, P. R., Wood, E. F., Schaake, J. C., ... others (2003). Real-time and retrospective forcing in the North American Land Data Assimilation System (NLDAS) project. *Journal of Geophysical Research: Atmospheres*, *108*(D22).

Endo, S., Fridlind, A. M., Lin, W., Vogelmann, A. M., Toto, T., Ackerman, A. S., ... Liu, Y. (2015). RACORO continental boundary layer cloud investigations: 2. Large-eddy simulations of cumulus clouds and evaluation with in situ and ground-based

observations. *Journal of Geophysical Research: Atmospheres*, *120* (12), 5993-6014.

Gustafson, W., Vogelmann, A., Cheng, X., Dumas, K., Endo, S., Johnson, K., . . . Xiao, H. (2019). Description of the LASSO data bundles product. DOE Atmospheric Radiation Measurement (ARM) user facility. *DOE/SC-ARM-TR-216*.

Gustafson, W. I., Vogelmann, A. M., Li, Z., Cheng, X., Dumas, K. K., Endo, S., . . . Xiao, H. (2020). The Large-eddy simulation (LES) Atmospheric Radiation Measurement (ARM) Symbiotic Simulation and Observation (LASSO) activity for continental shallow convection. *Bulletin of the American Meteorological Society*, *101* (4), E462–E479.

Homer, C. H., Fry, J. A., & Barnes, C. A. (2012). The national land cover database. *US Geological Survey Fact Sheet*, *3020* (4), 1–4.

Lin, Y., & Mitchell, K. E. (2005). The NCEP stage II/IV hourly precipitation analyses: Development and applications. In *Proceedings of the 19th conference hydrology, american meteorological society, san diego, ca, usa* (Vol. 10).

Mitchell, K. E., Lohmann, D., Houser, P. R., Wood, E. F., Schaake, J. C., Robock, A., . . . others (2004). The multi-institution North American Land Data Assimilation System (NLDAS): Utilizing multiple GCIP products and partners in a continental distributed hydrological modeling system. *Journal of Geophysical Research: Atmospheres*, *109* (D7).

Niu, G.-Y., Yang, Z.-L., Mitchell, K. E., Chen, F., Ek, M. B., Barlage, M., . . . others (2011). The community Noah land surface model with multiparameterization options (Noah-MP): 1. model description and evaluation with local-scale measure-

ments. *Journal of Geophysical Research: Atmospheres*, *116*(D12).

Simon, J. S., Bragg, A. D., Dirmeyer, P. A., & Chaney, N. W. (2021). Semi-coupling of
a field-scale resolving land-surface model and wrf-les to investigate the influence of
land-surface heterogeneity on cloud development. *Journal of Advances in Modeling
Earth Systems*, *13*(10), e2021MS002602.

Skamarock, W., Klemp, J., Dudhia, J., Gill, D., Barker, D., Duda, M., ... Powers, J.
(2008). A description of the Advanced Research WRF version 3. *NCAR Technical
Note, NCAR/TN-475+STR*.

Vergopolan, N., Chaney, N. W., Beck, H. E., Pan, M., Sheffield, J., Chan, S., & Wood,
E. F. (2020). Combining hyper-resolution land surface modeling with SMAP bright-
ness temperatures to obtain 30-m soil moisture estimates. *Remote Sensing of Envi-
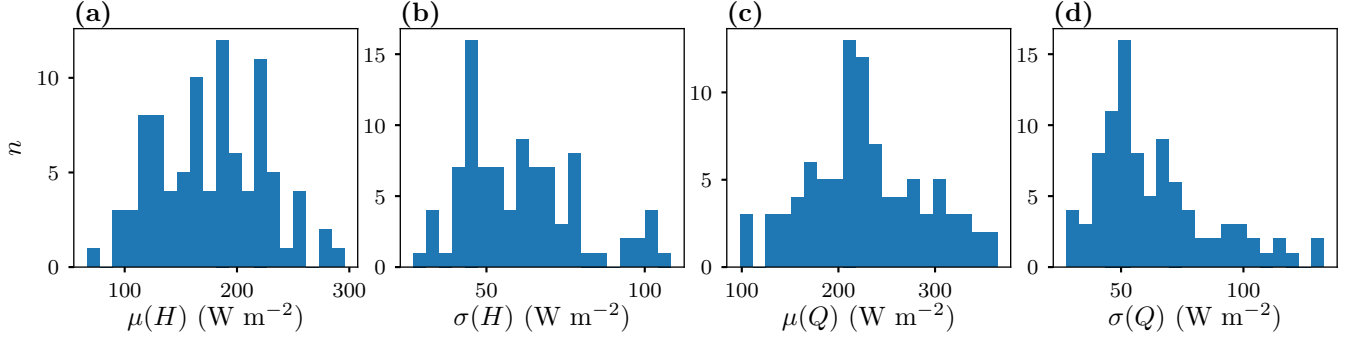ronment*, *242*, 111740.

Figure S1. Histogram of mean (μ) and standard deviation (σ) for mid-day sensible (H) and latent (Q) heat flux fields for the 92 cases.
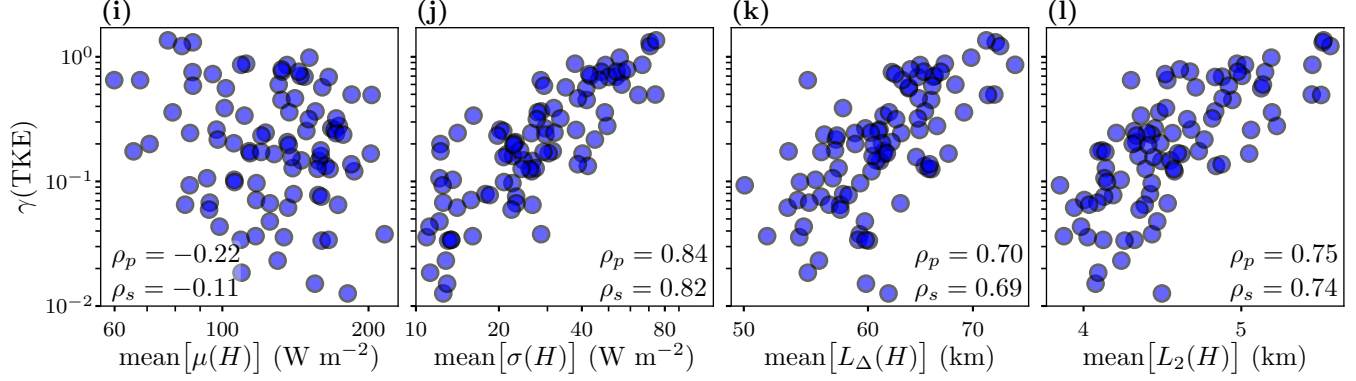

Figure S2. The $\gamma(\mathrm{TKE})$ metric as functions of statistics of the surface sensible heat flux field, H. One negative-valued data point for $\gamma(\mathrm{TKE})$ with a magnitudes $\mathcal{O}(10^{-2})$ is not shown, but is included in the calculation of ρ_p and ρ_s.
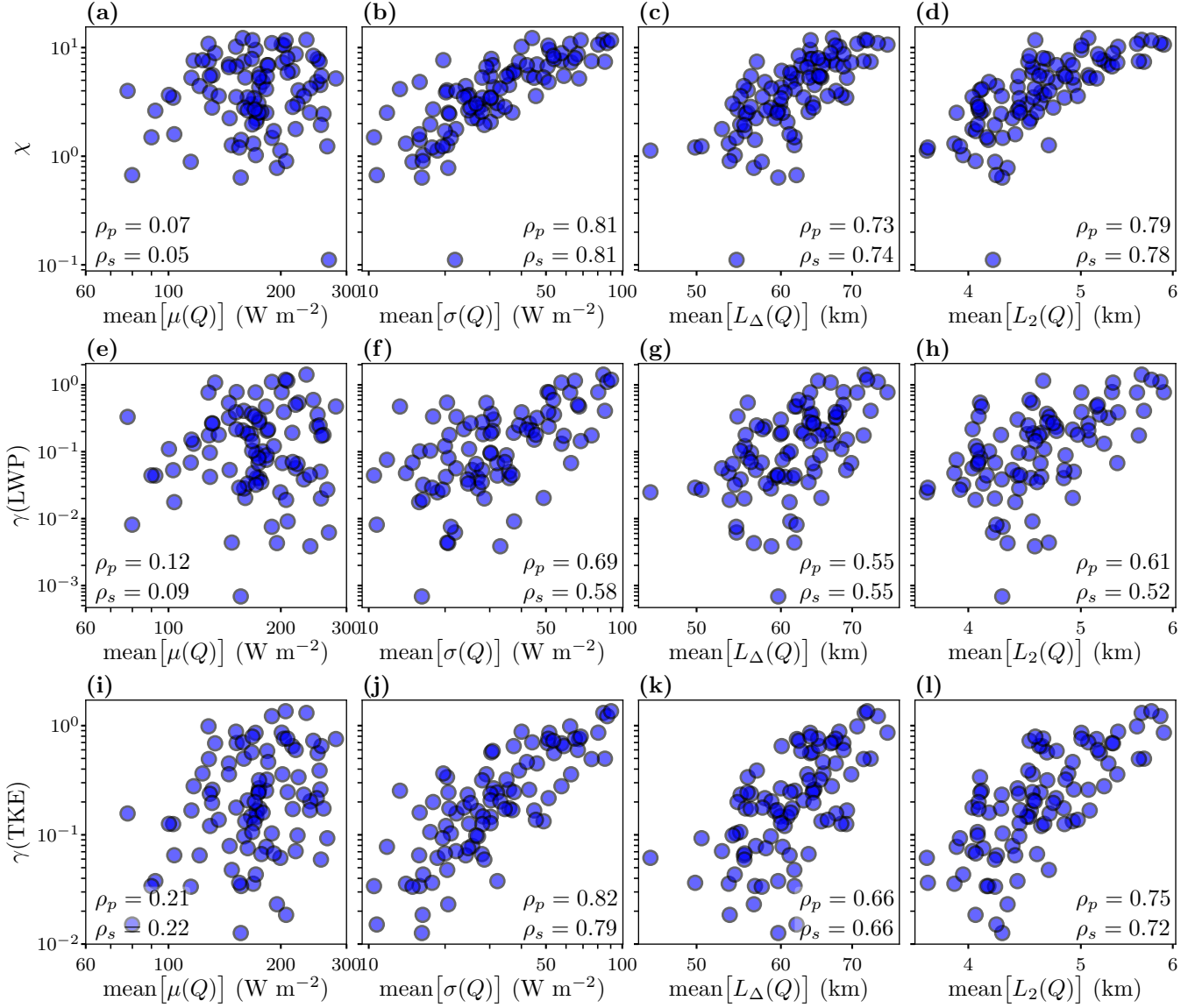
Figure S3. The χ (a – d), γ(LWP) (e – h), γ(TKE) (i – l) and metrics as functions of statistics of the surface latent heat flux field, Q.
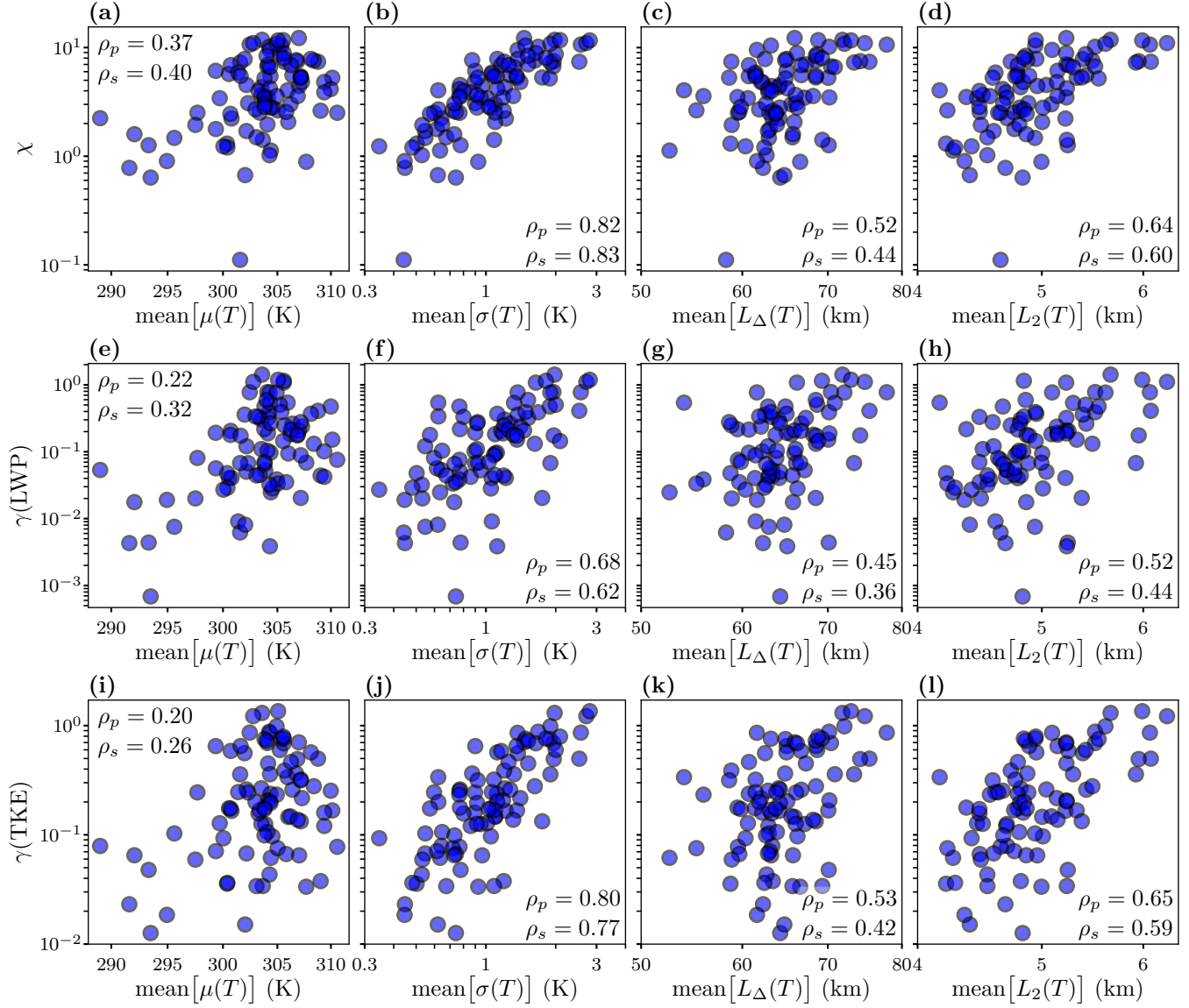
Figure S4. The χ (a – d), γ(LWP) (e – h), γ(TKE) (i – l) and metrics as functions of

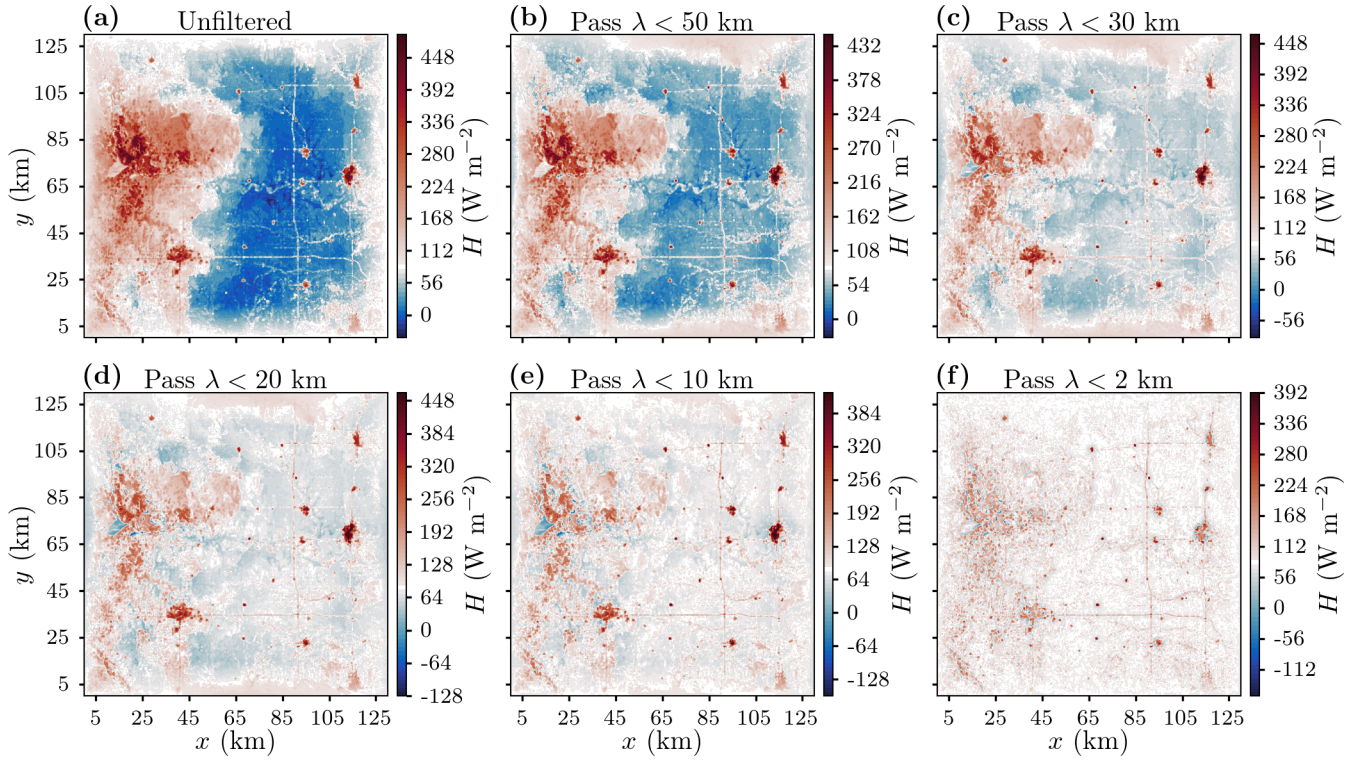statistics of the surface temperature field, T.

Figure S5. Comparison of a mid-day sensible heat flux field without filtering (a) and after applying increasingly fine filters (b – f).